Calculation of electron transport in multiterminal systems using complex absorbing potentials

Brandon G. Cook, Peter Dignard, and Kálmán Varga
Department of Physics and Astronomy, Vanderbilt University, Nashville, Tennessee 37235, USA
(Received 17 January 2011; revised manuscript received 28 February 2011; published 16 May 2011)

A method to calculate the transmission coefficient in multiterminal systems is presented. By adding a complex absorbing potential to the Hamiltonian of the semi-infinite leads, the problem of inverting an infinite dimensional matrix is transformed into a finite dimensional eigenvalue problem. Using this approach transmission coefficients are calculated for all energies at once. The accuracy of the approach is demonstrated with an analytically solvable model system. Numerical examples of a four-terminal graphene cross junction and six-terminal carbon nanotube junction are presented.

DOI: 10.1103/PhysRevB.83.205105 PACS number(s): 73.40.−c, 73.63.−b, 72.10.−d, 85.65.+h

I. INTRODUCTION

Many properties of nanomaterials can be explored by studying electron-transport processes.[1,2] In a typical transport measurement the sample is contacted by two probes and the conductance or current-voltage characteristics is measured.[3] Three- and four-probe measurements are also becoming common.[4–6] These multiprobe experiments allow researchers to study quantum interference effects, local currents, switching mechanisms, and other unique properties that are beyond the reach of two-probe measurements.

Electron-transport calculations in two-terminal nanodevices have been rapidly developing ever since the first transport measurements. Due to the simplicity of the formulation, the nonequilibrium Green's function (NEGF) approach using density functional theory's (DFT) Kohn-Sham Hamiltonian became a popular approach to calculate transport properties of nanostructures.[7–17]

Computational approaches for three- and four-terminal calculations have recently become available.[21–31] The first multiterminal calculations used tight-binding Hamiltonians[21,29–31] and only a few first-principles calculations exist.[23,27] These calculations use the NEGF formalism extended to the three- and four-terminal case. The extension of the NEGF formalism to four-terminal devices is straightforward but tedious. In the case of the two-terminal NEGF, the Hamiltonian of the system is infinite dimensional, but it has a block tridiagonal matrix structure which allows for efficient evaluation of the Green's function for each energy point. In the four-terminal case the structure of the Hamiltonian matrix is more complicated,[23] and while the matrix is still sparse with nonzero block matrices, the calculation of its inverse is more difficult. The extension to more than four terminals is possible but the calculation becomes even more complex.

We have recently developed a complex potential quantum transport framework.[32,33] In this approach complex absorbing potentials (CAPs) are added to the Hamiltonian in the leads. The complex absorbing potentials transform the infinite open system into a finite closed system by effectively cutting the leads off at a finite distance from the central region. The results of this approach are in excellent agreement with the nonequilibrium Green's function calculations[33] but with much less computational effort because the evaluation of the Green's functions of the infinite leads is avoided.

In this paper we extend the CAP approach to multiterminal devices. In the multiterminal case, a CAP will be added to the Hamiltonian of each lead and the transmission coefficients will be calculated by using a transmission formula that is generalized for the multiterminal case. The main advantage of the approach, as in the two-terminal case, is that one can deal with finite dimensional matrices instead of infinite dimensional ones. Another advantage is the simplicity of the implementation, which allows the approach to be easily extended for N-terminal junctions.

Analytically solvable systems with four and eight terminals are examined to demonstrate the accuracy of the approach. We also present calculations of a four-terminal graphene cross junction and a six-terminal carbon nanotube junction to show the efficiency of the approach.

The outline of this paper is as follows. After this introduction we present the formalism used in the calculations of Sec. II. In Sec. III numerical examples are presented. The paper ends with a brief summary in Sec. IV. Additional details are presented in four appendices: elements of formal scattering theory, simplification of the expression of the transmission coefficient, the transmission coefficient with CAP, and an analytical solution for a four-terminal device.

II. FORMALISM

A. Basis function representation of the Hamiltonian

We consider the multiterminal device structure shown in Fig. 1, where localized basis functions will be used to represent the Hamiltonian of the system. Various localized basis function sets have been tested in transport calculations, including localized atomic orbitals[7–17] and box basis functions.[34] The localized basis functions overlap with each other only in a given region, leading to sparse Hamiltonian and overlap matrices. In the present work each lead and the central region has its own set of basis functions. The range of overlap is restricted in such a way that there is no overlap between the basis functions of different leads, but there is an overlap between some of the basis functions of the central region and leads.

The leads consist of periodically repeated cells. The size of the cells is chosen such that the basis functions connect only

 ©2011 American Physical Society

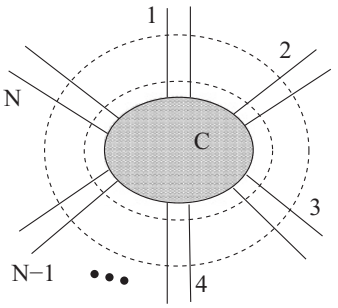

FIG. 1. *N*-terminal junction. The CAP is added between the two dashed lines and the shaded area represents the center region.

the neighboring cells and the Hamiltonian matrix of lead a has a block-tridiagonal structure:

$$H_a = \begin{pmatrix} h_a^{00} & h_a^{10+} & 0 & 0 \\ h_a^{10} & h_a^{00} & h_a^{10+} & 0 \\ 0 & h_a^{10} & h_a^{00} & \dots \\ 0 & 0 & \dots & \dots \end{pmatrix}. \tag{1}$$

The overlap matrix of lead a is

$$S_a = \begin{pmatrix} s_a^{00} & s_a^{10+} & 0 & 0 \\ s_a^{10} & s_a^{00} & s_a^{10+} & 0 \\ 0 & s_a^{10} & s_a^{00} & \dots \\ 0 & 0 & \dots & \dots \end{pmatrix}. \tag{2}$$

Denoting the Hamiltonian matrices coupling lead a and the central region by τ_a and the Hamiltonian of the central region by H_C, the Hamiltonian of the N-terminal system takes the form

$$\boldsymbol{H} = \begin{pmatrix} H_1 & 0 & \dots & 0 & 0 & \tau_1^+ \\ 0 & H_2 & \dots & 0 & 0 & \tau_2^+ \\ \vdots & \vdots & \ddots & \vdots & \vdots & \vdots \\ 0 & 0 & \dots & H_{N-1} & 0 & \tau_{N-1}^+ \\ 0 & 0 & \dots & 0 & H_N & \tau_N^+ \\ \tau_1 & \tau_2 & \dots & \tau_{N-1} & \tau_N & H_C \end{pmatrix}. \tag{3}$$

Bold fonts indicate that the quantity has dimensions of the full system.

B. Transmission in a multiterminal system

In this section we show how to calculate the transmission coefficient of the electron transport from lead a to lead b. The derivation is based on multichannel scattering theory.[35] To make the paper self-contained, the most important equations of multichannel scattering theory are summarized in Appendix A.

The wave function of the system corresponding to the partition shown in Fig. 1 is

$$\boldsymbol{\Psi} = \begin{pmatrix} \psi_1 \\ \psi_2 \\ \vdots \\ \psi_{N-1} \\ \psi_N \\ \psi_C \end{pmatrix}. \tag{4}$$

The wave function of the isolated lead a ($a = 1,\dots N$) is

$$\boldsymbol{\Phi}_a = \begin{pmatrix} 0 \\ \vdots \\ 0 \\ \phi_a \\ 0 \\ \vdots \\ 0 \end{pmatrix}, \tag{5}$$

where ϕ_a is the eigenfunction of the Hamiltonian of lead a,

$$H_a\phi_a = E_a\phi_a. \tag{6}$$

The wave function with incoming asymptotic form in lead a is

$$\boldsymbol{\Psi}_a^+ = [\mathbf{1} + \boldsymbol{G}(E_a + i\epsilon)\boldsymbol{V}_a]\,\boldsymbol{\Phi}_a, \tag{7}$$

where

$$\boldsymbol{G}(E + i\epsilon) = \frac{1}{(E + i\epsilon)\mathbf{1} - \boldsymbol{H}}, \tag{8}$$

and

$$\boldsymbol{V}_a = \begin{pmatrix} 0 & \dots & 0 & 0 & 0 & \dots & 0 & 0 \\ \vdots & \ddots & \vdots & \vdots & \vdots & \ddots & \vdots & \vdots \\ 0 & \dots & 0 & 0 & 0 & \dots & 0 & 0 \\ 0 & \dots & 0 & \tau_a & 0 & \dots & 0 & 0 \end{pmatrix}. \tag{9}$$

Similarly, the wave function with outgoing asymptotic form in lead b is given by

$$\boldsymbol{\Psi}_b^- = [\mathbf{1} + \boldsymbol{G}(E_b - i\epsilon)\boldsymbol{V}_b]\boldsymbol{\Phi}_b. \tag{10}$$

The transmission probability from lead b to lead a can be calculated from

$$|\langle\boldsymbol{\Psi}_b^-|\boldsymbol{\Psi}_a^+\rangle|^2, \tag{11}$$

which can be rewritten as (see Appendix A)

$$|\langle\boldsymbol{\Phi}_b|\boldsymbol{V}_b(\mathbf{1} + \boldsymbol{G}(E)\boldsymbol{V}_a)|\boldsymbol{\Phi}_a\rangle|^2 = |\langle\boldsymbol{\Phi}_b|\boldsymbol{V}_b\boldsymbol{G}(E)\boldsymbol{V}_a|\boldsymbol{\Phi}_a\rangle|^2, \tag{12}$$

where in writing the second equality we have used the fact that V_b does not connect leads a and b,

$$\langle \mathbf{\Phi}_b | V_b | \mathbf{\Phi}_a \rangle = 0. \tag{13}$$

To calculate the transmission from lead b to lead a we have to sum over all lead wave functions:

$$\begin{aligned} T_{ab}(E) &= \sum_{\alpha\beta} \left| \left\langle \mathbf{\Phi}_b^\beta \middle| V_b \boldsymbol{G}(E) V_a \middle| \mathbf{\Phi}_a^\alpha \right\rangle \right|^2 = \sum_{\alpha\beta} \left\langle \mathbf{\Phi}_b^\beta \middle| V_b \boldsymbol{G}(E) V_a \middle| \mathbf{\Phi}_a^\alpha \right\rangle \left\langle \mathbf{\Phi}_a^\alpha \middle| V_a^+ \boldsymbol{G}(E)^+ V_b \middle| \mathbf{\Phi}_b^\beta \right\rangle \\ &= \sum_{\beta} \left\langle \mathbf{\Phi}_b^\beta \middle| V_b \boldsymbol{G}(E) \mathbf{\Gamma}_a \boldsymbol{G}(E)^+ V_b^+ \middle| \mathbf{\Phi}_b^\beta \right\rangle = \sum_{\beta} \sum_{k} \left\langle \mathbf{\Phi}_b^\beta \middle| V_b | \boldsymbol{k} \right\rangle \langle \boldsymbol{k} | \boldsymbol{G}(E) \mathbf{\Gamma}_a \boldsymbol{G}(E)^+ V_b^+ \middle| \mathbf{\Phi}_b^\beta \rangle \\ &= \sum_{k} \langle \boldsymbol{k} \middle| \boldsymbol{G}(E) \mathbf{\Gamma}_a \boldsymbol{G}^+(E) \mathbf{\Gamma}_b \middle| \boldsymbol{k} \rangle = \mathrm{Tr}[\boldsymbol{G}(E) \mathbf{\Gamma}_a \boldsymbol{G}(E)^+ \mathbf{\Gamma}_b]. \end{aligned} \tag{14}$$

In the above equations we have introduced the notation

$$\mathbf{\Gamma}_a = V_a^+ \left(\sum_\alpha \left| \mathbf{\Phi}_a^\alpha \right\rangle \left\langle \mathbf{\Phi}_a^\alpha \right| \right) V_a, \tag{15}$$

and $|\boldsymbol{k}\rangle$ stands for a complete set of states formed by superposing all lead bases.

In Eq. (14) the transmission coefficient is expressed by the Green's function of the whole system and by the $\mathbf{\Gamma}$ matrices. While the Hamiltonian of the system is a sparse block structured matrix, the Green's function matrix is not sparse. The sparse structure of the $\mathbf{\Gamma}$ matrix, however, allows for the simplification of the transmission coefficient. As shown in Appendix B, the transmission coefficient can be rewritten as

$$T_{ab}(E) = \mathrm{Tr}[G_C(E) \Gamma_a G_C(E)^+ \Gamma_b], \tag{16}$$

where G_C is the Green's function of the central region and Γ_a and Γ_b are the imaginary parts of the self-energies of leads a and b. This expression is the transmission coefficient used in two-terminal transport calculations.[36,37] In the present work we will add a CAP to the Hamiltonian of the leads and both Eqs. (14) and (16) will be used in the calculations. The addition of the CAP is described in the next section.

C. Complex absorbing potentials

Absorbing boundary conditions by using CAPs was first introduced in time-dependent quantum mechanical calculations to avoid artificial reflections caused by the use of finite basis sets or grids.[38] These CAPs are located in the asymptotic region and annihilate the outgoing waves preventing the undesired reflections. CAPs are extensively used in quantum mechanical calculations of chemical reaction rates and in time-dependent wave-packet calculations.[39–45] Complex potentials have also been used in transport calculations.[46,47]

The complex potentials not only absorb the outgoing waves but can also produce reflections themselves. The construction and optimization of reflection-free CAPs is therefore pursued by many research groups. Many different forms of pure imaginary potential have been investigated, including linear, power-law,[40,42] polynomial,[43] and other parameterized functional forms (a recent review is provided by Muga *et al.*[41]). Besides purely imaginary potentials, complex potentials have also been investigated.[44] In this work we will adopt the CAP suggested by Manolopoulos.[45] This negative, imaginary CAP is derived from a physically motivated differential equation and its form is

$$-i\,w(x) = -i \frac{\hbar^2}{2m} \left(\frac{2\pi}{\Delta x} \right)^2 f(y), \tag{17}$$

where x_1 is the start and x_2 is the end of the absorbing region (see Fig. 1), $\Delta x = x_2 - x_1$, c is a numerical constant, m is the electron's mass, and

$$f(y) = \frac{4}{c^2} \left(\frac{1}{(1+y)^2} + \frac{1}{(1-y)^2} - 2 \right), \quad y = \frac{(x - x_1)}{\Delta x}. \tag{18}$$

This CAP goes to infinity at the end of the absorbing region and is therefore exactly transmission free. The CAP contains only one parameter, the width of the absorbing region Δx. Its reflection properties are guaranteed to improve as this parameter is increased.

By adding the CAP [as defined in Eqs. (17) and (18)] to the Hamiltonian of lead j one obtains

$$H_j' = H_j + i W_j \tag{19}$$

where W_j contains the matrix elements of the complex potential on the left and the right. Assuming that the basis states connect only the neighboring cells in the lead, these matrices will have the same block tridiagonal structure as the leads' Hamiltonian, but for the nonperiodic CAP the matrices in the diagonals will not be identical:

$$W_j = \begin{pmatrix} w_j^{00} & w_j^{10+} & 0 & 0 \\ w_j^{10} & w_j^{11} & w_j^{21+} & 0 \\ 0 & w_j^{21} & w_j^{22} & \dots \\ 0 & 0 & \dots & \dots \end{pmatrix}. \tag{20}$$

The addition of a CAP makes the Hamiltonian a finite dimensional matrix; beyond the range of the complex potential, the lead is effectively cut off. In the calculations we assume that the complex potential starts at least one lead cell away from the central region (see Fig. 1). With this choice, assuming that the basis functions in the leads only connect neighboring supercells, the τ_i coupling matrices will not have contributions from the complex potential. The Hamiltonian of the system is now

$$\boldsymbol{H}' = \begin{pmatrix} H_1 + iW_1 & 0 & \dots & 0 & 0 & \tau_1^+ \\ 0 & H_2 + iW_2 & \dots & 0 & 0 & \tau_2^+ \\ \vdots & \vdots & \ddots & \vdots & \vdots & \vdots \\ 0 & 0 & \dots & H_{N-1} + iW_{N-1} & 0 & \tau_{N-1}^+ \\ 0 & 0 & \dots & 0 & H_N + iW_N & \tau_N^+ \\ \tau_1 & \tau_2 & \dots & \tau_{N-1} & \tau_N & H_C \end{pmatrix}. \tag{21}$$

The addition of a CAP modifies only the wave functions and the Green's functions in the region where the CAP is nonzero.[33] In the central region the electron density and the transmission probability are the same as one would obtain using semi-infinite leads without the CAP. The accuracy of the CAP approach in transport calculations has been demonstrated.[33] The transport coefficients calculated by the CAP approach are in excellent agreement with the results of conventional calculations using decimation or iteration[48,49] to calculate the Green's function of the leads.

In the CAP formalism, the transmission probability can be calculated by using Eq. (14) or (16). In the first approach, Eq. (14) can be rewritten as (see Appendix C)

$$T_{ab}(E) = 4\mathrm{Tr}\left[\boldsymbol{G}'(E)\mathbf{W}_a\boldsymbol{G}'(E)^+\mathbf{W}_b\right]. \tag{22}$$

To calculate the transmission coefficients in many energy points one has to recalculate the inverse $\boldsymbol{G}' = (E\boldsymbol{I} - \boldsymbol{H}')^{-1}$ for each energy point. To calculate this inverse one can solve the eigenvalue problem of the complex symmetric matrix $\boldsymbol{H}'$,

$$\boldsymbol{H}'C_k = \left(E_k - \frac{i}{2}\Delta_k\right)C_k, \tag{23}$$

where E_k and Δ_k are the real and imaginary parts of the eigenvalues. The spectral decomposition of the Green's matrix is now

$$\boldsymbol{G}'(E) = \sum_k \frac{C_k C_k^T}{E - E_k + \frac{i}{2}\Delta_k}. \tag{24}$$

In this way only one diagonalization is needed and the Green's function is available for any energy at once. The dimension of the Hamiltonian is large, but it is a sparse matrix so efficient diagonalization algorithms can be used. One can also truncate the expansion using only the eigenfunctions with a real part of the energy below a preset energy maximum. Numerical tests show that high-lying states do not contribute to the spectral decomposition in the desired energy range around the Fermi energy. One should also note that if the size of the Hamiltonian matrix does not allow direct diagonalization then one can use recursive methods, for example, those based on damped Chebyshev polynomial expansions[50–52] or the Lanczos algorithm.[53,54]

Using the spectral representation, one can rewrite the transmission coefficient in an explicitly energy-dependent simple form:

$$T_{ab}(E) = \sum_{ij} \frac{1}{E - E_i}\frac{1}{E - E_j^*}\boldsymbol{U}_{ij}^a\boldsymbol{U}_{ij}^b \tag{25}$$

where

$$\boldsymbol{U}_{ij}^n = \sum_{kl} C_{ki}(\mathbf{W}_n)_{kl}C_{lj}^*. \tag{26}$$

This form again shows that once the eigenvalue problem is solved, the transmission coefficient is available for any energy.

Alternatively, one can use Eq. (16) to calculate the transmission coefficient. In that case, the Green's function of each lead has to be calculated separately,

$$g_n'(E) = (ES_n - H_n')^{-1}. \tag{27}$$

Once the leads' Green's functions are available, the imaginary part of the leads' self-energy can be calculated and Eq. (16) can be used.

In a zero bias (equilibrium) case, the electron density can be calculated in the conventional way using the imaginary part of the Green's function defined in Eq. (24). In a nonequilibrium case, the density can be calculated as

$$\rho(\mathbf{r}) = \sum_{\mu,\nu} \phi_\mu^*(\mathbf{r})\mathrm{Re}[\boldsymbol{D}_{\mu\nu}]\phi_\nu(\mathbf{r}), \tag{28}$$

where ϕ_ν are basis functions and $\boldsymbol{D}$ is the density matrix defined by

$$\begin{aligned}\boldsymbol{D} &= \sum_b \frac{1}{2\pi}\int_{-\infty}^{+\infty} dE\boldsymbol{G}'(E)\mathbf{W}_b(E)\boldsymbol{G}'^\dagger(E)f(E-\mu_b) \\ &= -\frac{1}{\pi}\int_{-\infty}^{+\infty} dE\mathrm{Im}[\boldsymbol{G}'(E)f(E-\mu_a)] \\ &\quad + \frac{1}{2\pi}\sum_{b\neq a}\int_{-\infty}^{+\infty} dE[\boldsymbol{G}'(E)\mathbf{W}_b(E)\boldsymbol{G}'^\dagger(E)] \\ &\quad \times [f(E-\mu_b) - f(E-\mu_a)]. \end{aligned} \tag{29}$$

Using the spectral representation [Eq. (24)] the density matrix can be rewritten as

$$\begin{aligned}\boldsymbol{D}_{\nu\mu} &= -\frac{1}{\pi}\int_{-\infty}^{+\infty} dE\mathrm{Im}\left[\sum_k \frac{C_{\nu k}C_{\mu k}^*}{E - E_k + \frac{i}{2}\Delta_k}\right] f(E-\mu_a) \\ &\quad + \frac{1}{2\pi}\sum_{b\neq a}\int_{-\infty}^{+\infty} \\ &\quad \times dE\left[\sum_{ij}\frac{C_{\nu i}C_{\mu j}^*\boldsymbol{U}_{ij}^b}{\left(E - E_i + \frac{i}{2}\Delta_i\right)\left(E - E_j - \frac{i}{2}\Delta_j\right)}\right] \end{aligned}$$

$$\times [f(E-\mu_b) - f(E-\mu_a)]$$
$$= \mathrm{Im}\left[\sum_k C_{\nu k} C^*_{\mu k} p^a_k\right] + \sum_{b\neq a}\sum_{ij} C_{\nu i} C^*_{\mu j} U^b_{ij} q^{ab}_{ij} \quad (30)$$

where

$$p^a_k = -\frac{1}{\pi}\int_{-\infty}^{+\infty} dE \frac{1}{E - E_k + \frac{i}{2}\Delta_k} f(E-\mu_a), \quad (31)$$

and

$$q^{ab}_{ij} = \frac{1}{2\pi}\sum_{b\neq a}\int_{-\infty}^{+\infty} dE \frac{f(E-\mu_b) - f(E-\mu_a)}{\left(E - E_i + \frac{i}{2}\Delta_i\right)\left(E - E_j - \frac{i}{2}\Delta_j\right)}. \quad (32)$$

The integrals in Eqs. (31) and (32) can be calculated by numerical integration to desired accuracy.

D. Hamiltonian

Two different Hamiltonians are used in the calculations. The first is a simple tight-binding Hamiltonian defined as

$$H = \sum_i \epsilon_i |i\rangle\langle i| - t\sum_i \left(|i\rangle\langle i+1| + |i+1\rangle\langle i|\right). \quad (33)$$

The reason for using this simple Hamiltonian is that it allows us to compare the results with analytical calculations.

A more realistic model is based on a DFT Hamiltonian defined as

$$H_{KS} = -\frac{\hbar^2}{2m}\nabla_{\mathbf{r}} + V_A(\mathbf{r}) + V_H[\rho](\mathbf{r}) + V_{XC}[\rho](\mathbf{r}), \quad (34)$$

where $V_A(\mathbf{r})$ is the atomic potential, $V_H[\rho](\mathbf{r})$ is the Hartree potential, and $V_{XC}(\mathbf{r})$ is the exchange-correlation potential. The pseudopotential approach is used to represent the atomic potentials $V_A(\mathbf{r})$. The exchange-correlation potential $V_{XC}(\mathbf{r})$ is constructed using the local density approximation,[18] and the Hartree potential is calculated by solving the Poisson equation. The density ρ is calculated self-consistently using Eq. (28).

In the DFT case, atomic orbitals are used as basis functions and the matrix elements

$$H_{\mu\nu} = \langle\phi_\mu|H_{KS}|\phi_\nu\rangle \quad (35)$$
$$S_{\mu\nu} = \langle\phi_\mu|\phi_\nu\rangle \quad (36)$$

will be used to set up the Hamiltonian and overlap matrices. The calculation of the matrix elements and the self-consistent potential is the same as in the conventional two-terminal calculations.[19,20,33,34]

III. NUMERICAL RESULTS

In this section we present our numerical results to show the accuracy and the applicability of the CAP approach.

A. Simple four-terminal junction

As a first example we have calculated the transmission in the four-terminal device shown in Fig. 2. The system will be described by a tight binding Hamiltonian (see Appendix D). The Hamiltonian of the leads is defined in Eq. (D3) with $V_i = 0$ and $t = 50$ (in atomic units). The Hamiltonian of the central region is defined in Eq. (D2) with $t = 50$ and $V_C = 10$ (in atomic units). This value for t corresponds to the values obtained with a three-point finite difference discretization with a step size of 0.1 atomic unit. The transmission coefficient calculated by using the CAP is compared to the analytical solution (presented in Appendix D) in Table I and in Fig. 3. Due to the symmetry of the Hamiltonian in this simple model, the transmission between any two leads is identical. Table I shows that the results of the CAP calculation are in excellent agreement with the analytical calculations. The agreement improves as the energy increases, because the CAP can more easily absorb the higher energy wave functions. The accuracy can be increased further by increasing the range of the CAP. Figure 3 shows that the transmission monotonically increases with energy. This is similar to the behavior of the transmission probability of a one-dimensional step barrier, where the transmission converges to 1 with increasing energy. In the four-terminal case the transmission converges to 1/4.

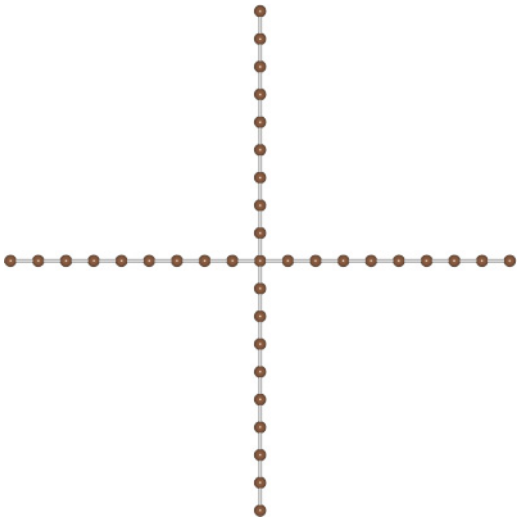

FIG. 2. (Color online) Four-terminal junction.

B. Eight-terminal junction

The next analytically solvable example is the eight-terminal junction shown in Fig. 4. The crossing points A, B, C, and D are separated by 21 sites. The same Hamiltonian is used as in the previous example, except that $V_C = 0$ is used in the present case. Thus the scattering in the eight-terminal junction

TABLE I. Transmission in four-terminal junctions. The energy is in atomic units.

E	CAP	Analytical
0.0	0.000 465	0.000 096
0.1	0.110 523	0.109 824
0.2	0.151 629	0.151 405
0.3	0.173 274	0.173 261
0.4	0.186 677	0.186 729
0.5	0.195 814	0.195 856
1.0	0.216 982	0.216 996
1.5	0.225 005	0.225 001
2.0	0.229 159	0.229 155

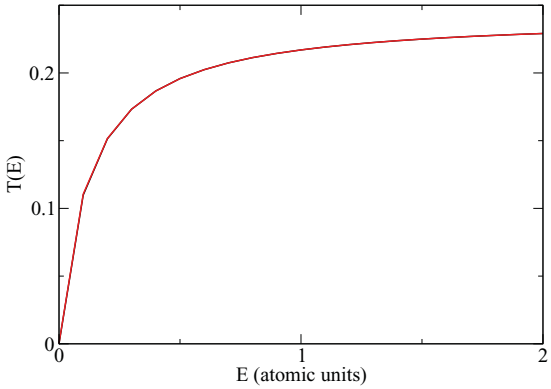

FIG. 3. (Color online) Transmission in a four-terminal junction. The results of the CAP and the analytical calculation are in complete agreement and cannot be distinguished in the resolution of the figure.

is purely due to the cross points. In the eight-terminal example, there are three different transmission coefficients T_{12}, T_{14}, and T_{15} (connecting lead 1 to leads 2, 4, and 5; see Fig. 4), all other transmissions are equal to these three due to the symmetry of the Hamiltonian. Figures 5 and 6 show the transmission coefficients calculated by using the CAP and by the analytical solution. The results of the CAP and analytical approaches are in perfect agreement.

Figure 5 shows the transmission between leads 1 and 2, T_{12}. This transmission is much larger than the other two transmissions T_{14} and T_{15} (see Fig. 6). This not surprising, because these two leads are directly connected and the there is only one scattering center between the two leads. The transmission oscillates around $5/16$ with an amplitude of $4/16$. This oscillation is due to the interference between the waves that directly scatter from 1 to 2 and those that go around the square and get backscattered from the vertices A, B, C, and D. The frequency of the oscillation increases with the distance between crossing points, because the energy spacing of the standing waves between crossing points decreases and more and more standing waves contribute to the interference.

Figure 6 shows the transmission coefficients T_{14} and T_{15}. These transmissions behave similarly to T_{12}, oscillating around $1/16$. The interference effect causes a very interesting

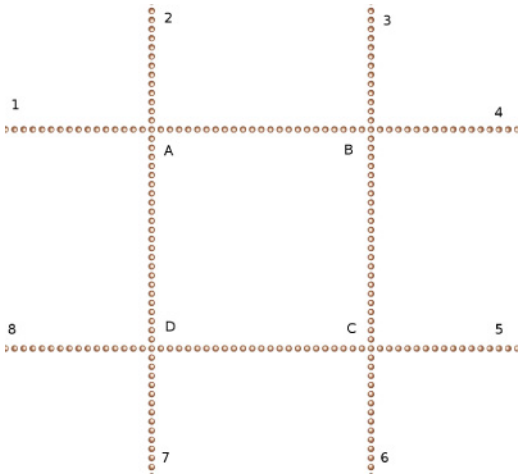

FIG. 4. (Color online) Eight-terminal junction.

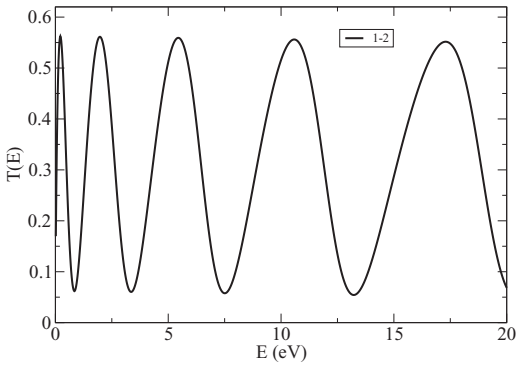

FIG. 5. Transmission (T_{12}) in an eight-terminal junction. The results of the CAP and the analytical calculation are in complete agreement and cannot be distinguished in the resolution of the figure.

behavior: in certain energy regions the transmission from 1 to 5 is larger than the transmission from 1 to 4, which is along a straight line. The period of oscillations, similar to the previous case, depends on the distance between the crossing points.

C. Four-terminal graphene device

The first realistic example using a self-consistent density functional Hamiltonian is a four-terminal graphene cross junction. A cross junction consists of an intersection between armchair and zigzag graphene ribbons. The geometry of the device is shown in Fig. 7. The region within the dotted box is the scattering region of the device. The armchair leads are $n_a = 8$ unit cells wide and the zigzag leads are $n_z = 6$ unit cells in width. Matrix elements are calculated with density functional theory using an atomic orbital basis set as described in Sec. II D.

In contrast to the simple devices discussed previously, with the graphene device there are more unique values for the transmission coefficients between leads. This is caused by the broken symmetry of the system at the corners of the cross region. However, the differences between the different values for turning a corner are small and similar behavior is observed. The calculated transmission is shown in Fig. 8. Our results are in agreement with the results of tight-binding calculations.[21] It is interesting to note that there is no gap for

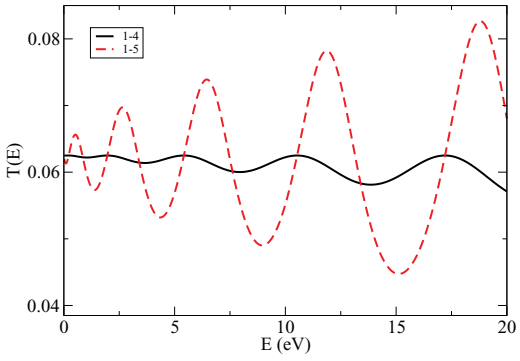

FIG. 6. (Color online) Transmission (T_{14} and T_{15}) in an eight-terminal junction. The results of the CAP and the analytical calculation are in complete agreement and cannot be distinguished in the resolution of the figure.

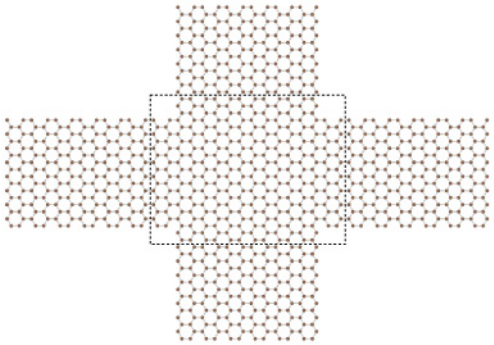

FIG. 7. (Color online) Graphene cross-junction device.

transmission between the two armchair leads but there is a gap for transmission between the two zigzag leads. A similar gap is found for the transmission between the two types of leads.

D. Six-terminal carbon nanotube junction

In this example a six-terminal junction built from three (5,0) semiconducting nanotubes with a density functional Hamiltonian is considered. Two tubes are placed parallel to each other. The third tube, oriented perpendicular to the other two, is placed on top as shown in Fig. 9. Ideal structures for the nanotubes are used in the work.

The transmission coefficients as a function of energy are shown in Figs. 10 and 11. Similar to the graphene case, the symmetry of the system is broken by the relative orientations of the nanotubes. That is, T_{24} is not the same as T_{35}. However, the two curves have similar features. Since the nanotubes in this configuration are loosely coupled, the transmission along the axis of any given nanotube is very similar to that through an isolated nanotube. Figure 10 shows that T_{23} and T_{16} both retain their semiconducting gap. The transmission along the two tubes is not the same, however, because one has two scattering centers and the other has only one. Due to the weak nature of the coupling, the transmission through leads on different tubes is significantly lower (see Fig. 10). The lowest transmission is seen to be from terminals 2 to 4, where the electron would have to go through all three tubes.

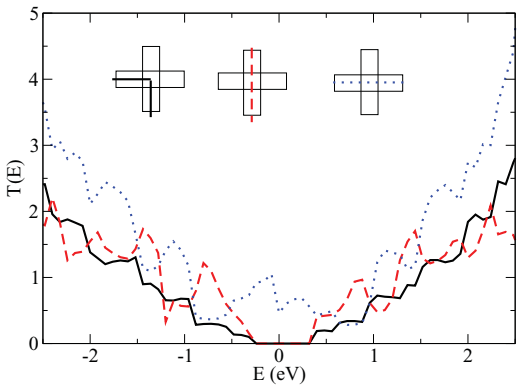

FIG. 8. (Color online) The transmission coefficient of a graphene cross-junction device.

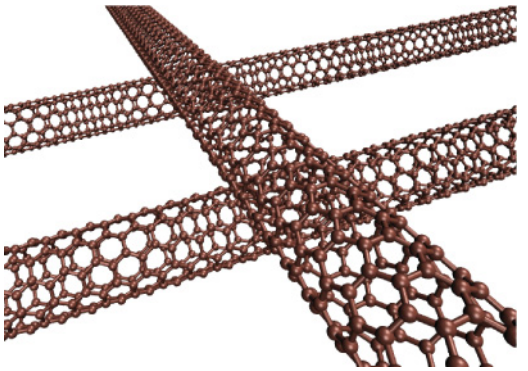

FIG. 9. (Color online) Six-terminal CNT junction.

E. Monoatomic gold chain cross

The last example is a calculation of the transmission and current-voltage characteristics for a monoatomic gold chain using a density functional Hamiltonian. The geometry of the system is the same as the four-terminal junction shown in Fig. 2. The gold atoms are placed 2.9 Å apart from each other. The calculated transmissions of the gold cross are shown in Fig. 12. The figure also shows the quantized transmission of the monoatomic gold chain for comparison. The transmission of the gold chain without the cross is $T(E) = nG_0$, where $G_0 = 2e^2/h$ is the unit of the quantum conductance and n is an integer which is equal to the number of Bloch states at a given energy E. Figure 12 shows that due to the scattering at the intersection of the two chains, the transmission in a straight line (T_{13}) of the cross is smaller than the transmission in the monoatomic chain (without a cross). In the simple tight-binding four-terminal case, T_{12} and T_{13} were equal to each other. In the gold cross case the right angle transmission T_{12} is much smaller than the straight line transmission. The variation of T_{13} and T_{12} follows the variation of the transmission of the monoatomic chain (with no cross). The self-consistent potential calculated for the gold junction is shown in Fig. 13. The figure shows that the potential distribution on the atom in the middle of the cross is different from the atoms in the chain. This difference is due to the fact that the middle atom has four neighbors while the other atoms have only two neighbors. This potential difference presents the perturbation leading to a reduction of transmission compared to the monoatomic case without a cross.

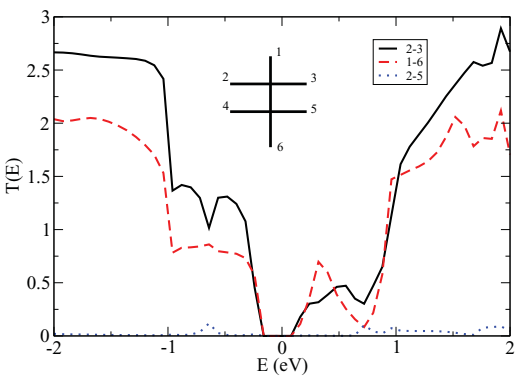

FIG. 10. (Color online) Transmission in a six-terminal CNT junction.

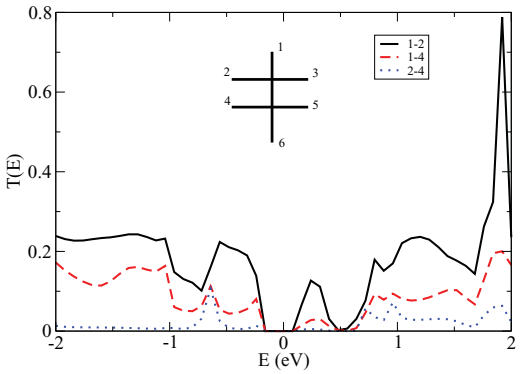

FIG. 11. (Color online) Transmission in a six-terminal CNT junction.

Next we show an example of an applied bias in the gold chain cross case. The complication in this case is that one has to solve the Poisson equation with proper boundary conditions to take into account the effect of the bias voltage applied on the leads. This problem has been solved in various ways in two-terminal calculations.[11,13] In a multiterminal case the solution is more complicated due to the larger number of leads and boundary conditions. In the present calculation we restrict ourself to the case where only two leads have bias voltage and there are no bias voltages on the rest of the leads. The implementation of the Poisson equation for more general cases is left for future work. Electrodes 1 and 3 (see Fig. 13) are connected to voltage $V_b/2$ and $-V_b/2$ and electrodes 2 and 4 have zero bias voltage. The self-consistent calculation is carried out in the same way as before, except that the nonequilibrium part of the density matrix also contributes to the density.

The current as a function of bias voltage is shown in Fig. 14. As one expects from the behavior of the transmission probability shown in Fig. 12, I_{13} is much larger than I_{12}. Further studies are needed to explore the dependence of the current flow on bias voltage on various leads, but this is out of the scope of the present work.

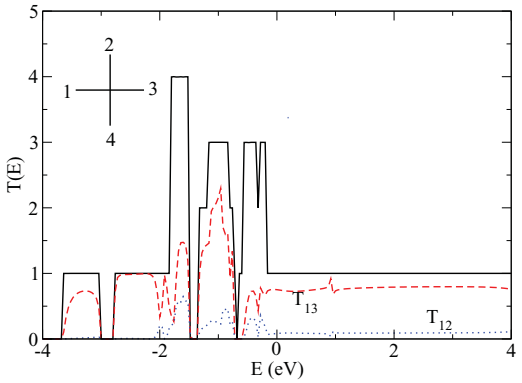

FIG. 12. (Color online) Transmission in a monoatomic gold chain cross. The transmission coefficients are calculated by both the CAP approach and by the conventional NEGF method using the decimation technique[48] to obtain the self-energies. The results of the two approaches are in complete agreement and cannot be distinguished in the resolution of the figure.

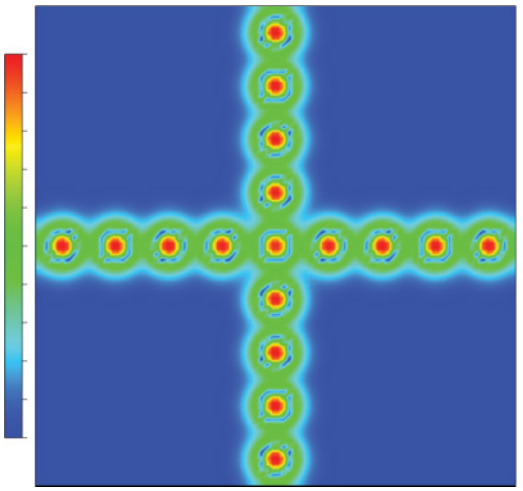

FIG. 13. (Color online) Potential distribution in a monoatomic gold chain cross.

IV. SUMMARY

We have presented an efficient and accurate way to calculate transmission coefficients in multiterminal systems using CAPs. By adding a complex absorbing potential to the Hamiltonian of the semi-infinite lead, the lead can be terminated in a finite distance leading to finite dimensional matrices. In this way the Green's function of the system can be calculated using a spectral representation for all energies at once. The test examples presented, including graphene and carbon nanotube multiterminal devices, show the accuracy and effectiveness of the approach.

The formalism presented in this paper is general and applies to systems with any number of terminals. To our knowledge, the details of the Green's function matrix formalism of the NEGF method has not been presented elsewhere for $N > 4$.

We have used a CAP which depends on only one parameter, its range, and its accuracy can be increased by increasing the range. This gives us a very effective way of controlling the convergence of the method. Calculations using other multiterminal systems are underway.

ACKNOWLEDGMENT

This work is supported by NSF Grant No. ECCS0925422.

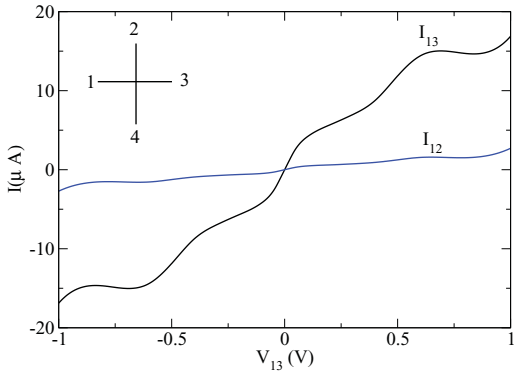

FIG. 14. (Color online) Current-voltage characteristics in the monoatomic gold chain cross.

APPENDIX A: ELEMENTS OF FORMAL SCATTERING THEORY

To make the paper self-contained, we briefly review some of the elements of the formal multichannel scattering theory used in the derivations. For more details refer to Ref. 35. A wave function in channel a is an eigenfunction of the channel Hamiltonian

$$H_a\phi_a = E_a\phi_a. \tag{A1}$$

These channel wave functions form a complete orthonormal set of states

$$\sum_\alpha |\phi_{a\alpha}\rangle\langle\phi_{a\alpha}| = 1. \tag{A2}$$

We can also define a Green's function for channel a

$$G_a(E_a + i\epsilon) = \frac{1}{E_a + i\epsilon - H_a}. \tag{A3}$$

The scattering wave function $\psi_a^\pm$ corresponding to the incoming or outgoing wave function from a satisfies

$$H\psi_a^\pm = E_a\psi_a^\pm. \tag{A4}$$

By combining these two equations one obtains the Lippmann-Schwinger equation for ψ_a^+,

$$\psi_a^+ = [1 + G(E_a + i\epsilon)V_a]\phi_a, \tag{A5}$$

where $+$ stands for an incoming wave boundary condition and

$$V_a = H - H_a. \tag{A6}$$

Similarly, an outgoing solution in channel b is given by

$$\psi_b^- = [1 + G(E_b - i\epsilon)V_b]\phi_b. \tag{A7}$$

One can define a transition matrix between a and b by

$$\mathcal{T}_{ba}^+\phi_a = V_b\psi_a^+ = [(V_b + V_bG(E_a + i\epsilon)V_a)]\phi_a. \tag{A8}$$

The transition probability from an incoming state in b to an outgoing state in a is given by

$$S_{ab}^2 = |\langle\boldsymbol{\psi}_b^-|\boldsymbol{\psi}_a^+\rangle|^2. \tag{A9}$$

By interchanging ψ_a^+ and ψ_b^-, the matrix element S_{ab} can be calculated from

$$S_{ab} = \delta_{ab} - 2\pi i\delta(E_a - E_b)\langle\phi_b|\mathcal{T}_{ab}|\phi_a\rangle. \tag{A10}$$

APPENDIX B: SIMPLIFICATION OF THE EXPRESSION FOR THE TRANSMISSION COEFFICIENT

The sparse block structure of the Hamiltonian matrix can be exploited to simplify the transmission coefficient [see Eq. (14)]. To calculate the Green's function matrix $\boldsymbol{G}$ one has to invert

$$E\boldsymbol{S} - \boldsymbol{H} = \begin{pmatrix} ES_1 - H_1 & 0 & \dots & 0 & 0 & \tau_1^+ \\ 0 & ES_2 - H_2 & \dots & 0 & 0 & \tau_2^+ \\ \vdots & \vdots & \ddots & \vdots & \vdots & \vdots \\ 0 & 0 & \dots & ES_{N-1} - H_{N-1} & 0 & \tau_{N-1}^+ \\ 0 & 0 & \dots & 0 & ES_N - H_N & \tau_N^+ \\ \tau_1 & \tau_2 & \dots & \tau_{N-1} & \tau_N & ES_C - H_C \end{pmatrix}. \tag{B1}$$

By defining

$$\tau = (\,\tau_1\ \tau_2\ \dots\ \tau_{N-1}\ \tau_N\,) \tag{B2}$$

and the block diagonal matrix

$$ES_L - H_L = \begin{pmatrix} ES_1 - H_1 & 0 & \dots & 0 & 0 \\ 0 & ES_2 - H_2 & \dots & 0 & 0 \\ \vdots & \vdots & \ddots & \vdots & \vdots \\ 0 & 0 & \dots & ES_{N-1} - H_{N-1} & 0 \\ 0 & 0 & \dots & 0 & ES_N - H_N \end{pmatrix} \tag{B3}$$

$E\boldsymbol{S} - \boldsymbol{H}$ can be rewritten in the following block form

$$E\boldsymbol{S} - \boldsymbol{H} = \begin{pmatrix} ES_L - H_L & \tau^+ \\ \tau & ES_C - H_C \end{pmatrix}. \tag{B4}$$

The inverse of this matrix can be calculated by partitioning[55]

$$\boldsymbol{G}(E) = (E\boldsymbol{S} - \boldsymbol{H})^{-1} = \begin{pmatrix} G_L(E) - [G_L(E)\tau^+]G_C(E)[\tau G_L(E)] & -[G_L(E)\tau^+]G_C(E) \\ -G_C(E)\,[\tau G_L(E)] & G_C(E) \end{pmatrix}. \tag{B5}$$

In the above equation we have introduced the Green's function of the center

$$G_C(E) = [ES_C - H_C - \tau G_L(E)\tau^+]^{-1} \tag{B6}$$

and the Green's function of the leads

$$G_L(E) = (ES_L - H_L)^{-1} = \begin{pmatrix} g_1 & 0 & \dots & 0 & 0 \\ 0 & g_2 & \dots & 0 & 0 \\ \vdots & \vdots & \ddots & \vdots & \vdots \\ 0 & 0 & \dots & g_{N-1} & 0 \\ 0 & 0 & \dots & 0 & g_N \end{pmatrix}, \tag{B7}$$

where the $g_i(E)$ matrices are the Green's functions of the leads,

$$g_i(E) = (ES_i - H_i)^{-1}. \tag{B8}$$

Using the Green's functions of the leads, the G_C matrix can also be simplified to

$$G_C(E) = \left[ES_C - H_C - \sum_{i=1}^{N} \Sigma_i(E) \right]^{-1} \tag{B9}$$

where

$$\Sigma_i(E) = \tau_i g_i(E) \tau_i^+. \tag{B10}$$

Now we can use these results to simplify the expression of the transmission coefficient in Eq. (14). In Eq. (14), the transmission coefficient

$$T_{ab}(E) = \sum_{\alpha\beta} \left| \langle \mathbf{\Phi}_b^\beta | \boldsymbol{V}_b \boldsymbol{G}(E) \boldsymbol{V}_a | \mathbf{\Phi}_a^\alpha \rangle \right|^2 \tag{B11}$$

can be simplified by using the equation

$$\langle \mathbf{\Phi}_b^\beta | \boldsymbol{V}_b \boldsymbol{G}(E) \boldsymbol{V}_a | \mathbf{\Phi}_a^\alpha \rangle = \langle \phi_b^\beta | \tau_b^+ G_C(E) \tau_a | \phi_a^\alpha \rangle \tag{B12}$$

which can be easily derived using Eqs. (B5), (5), and (9). Using this expression the derivation on Eq. (14) can be repeated and one obtains

$$\begin{aligned} T_{ab}(E) &= \sum_{\alpha\beta} \left| \langle \phi_b^\beta | \tau_b^+ G_C(E) \tau_a | \phi_a^\alpha \rangle \right|^2 \\ &= \sum_{\alpha\beta} \langle \phi_b^\beta | \tau_b G_C(E) \tau_a | \phi_a^\alpha \rangle \langle \phi_a^\alpha | \tau_a^+ G_C(E)^+ \tau_b | \phi_b^\beta \rangle \\ &= \sum_{\beta} \langle \phi_b^\beta | \tau_b G_C(E) \Gamma_a G_C(E)^+ \tau_b^+ | \phi_b^\beta \rangle \\ &= \sum_{\beta} \sum_{\beta'} \langle \phi_b^\beta | \tau_b | \beta' \rangle \langle \beta' | G_C(E) \Gamma_a G_C(E)^+ \tau_b^+ | \phi_b^\beta \rangle \\ &= \sum_{\beta'} \langle \beta' | G_C(E) \Gamma_a G_C(E)^+ \Gamma_b | \beta' \rangle \\ &= \mathrm{Tr}[G_C(E) \Gamma_a G_C(E)^+ \Gamma_b], \end{aligned} \tag{B13}$$

where

$$\begin{aligned} \Gamma_a &= \tau_a^+ \left(\sum_\alpha |\phi_a^\alpha\rangle\langle\phi_a^\alpha| \right) \tau_a \\ &= \tau_a^+ (g_a(E) - g_a(E)^+) \tau_a \\ &= i(\Sigma_a(E) - \Sigma_a(E)^+). \end{aligned} \tag{B14}$$

APPENDIX C: TRANSMISSION COEFFICIENT WITH CAPs

After the CAP is added to the Hamiltonian, the transmission coefficient can be calculated using Eq. (14),

$$T_{ab}(E) = \mathrm{Tr}[\boldsymbol{G}'(E) \boldsymbol{\Gamma}'_a \boldsymbol{G}'(E)^+ \boldsymbol{\Gamma}'_b]. \tag{C1}$$

In this equation the prime indicates that the CAP is added, that is, the Green's function is defined by

$$\boldsymbol{G}'(E) = (E\boldsymbol{S} - \boldsymbol{H}')^{-1}, \tag{C2}$$

where H' is defined in Eq. (21). In a manner corresponding to the partitioning of the Hamiltonian, the Green's function matrix can be partitioned as

$$\boldsymbol{G}' = (E\boldsymbol{S} - \boldsymbol{H}')^{-1} = \begin{pmatrix} G'_{11} & G'_{12} & \dots & G'_{1N} & G'_{1C} \\ G'_{21} & G'_{22} & \dots & G'_{2N} & G'_{2C} \\ \vdots & \vdots & \ddots & \vdots & \vdots \\ G'_{N1} & G'_{N2} & \dots & G'_{NN} & G'_{NC} \\ G'_{C1} & G'_{C2} & \dots & G'_{CN} & G'_{C} \end{pmatrix}. \tag{C3}$$

Using the result of Appendix B, the transmission can be rewritten as

$$T_{ab}(E) = \mathrm{Tr}[G'_C(E) \Gamma'_a G'_C(E)^+ \Gamma'_b] \tag{C4}$$

$$= \mathrm{Tr}[G'_C(E) \tau_a^+ (g'_a - g_a'^+) \tau_a G'_C(E) \tau_b^+ (g'_b - g_b'^+) \tau_b]. \tag{C5}$$

Using the identity

$$i(g'_a - g_a'^+) = i g'_a \left(g_a'^{+-1} - g_a'^{-1} \right) g_a'^{+} = 2 g'_a W_a g_a'^{+} \tag{C6}$$

one has

$$T_{ab}(E) = 4\mathrm{Tr}[G'_C(E) \tau_a g'_a W_a g_a'^+ \tau_a G'_C(E) \tau_b g'_b W_b g'_b \tau_b]. \tag{C7}$$

One can notice that in this equation we have

$$G'_{ab} = g'_a \tau_a^+ G'_C \tau_b g'_b. \tag{C8}$$

Using this the transmission becomes

$$\begin{aligned} T_{ab}(E) &= 4\mathrm{Tr}[G'_{ab} W_a G'^{+}_{ab} W_b] \\ &= 4\mathrm{Tr}\left[\boldsymbol{G}' \boldsymbol{W}_a \boldsymbol{G}^+ \boldsymbol{W}_b \right] \end{aligned} \tag{C9}$$

where

$$\boldsymbol{W}_i = \begin{pmatrix} 0 & 0 & \dots & 0 & 0 \\ \vdots & \vdots & \ddots & \vdots & \vdots \\ 0 & 0 & \dots & 0 & 0 \\ 0 & 0 & W_i & 0 & 0 \\ 0 & 0 & \dots & 0 & 0 \\ \vdots & \vdots & \ddots & \vdots & \vdots \\ 0 & 0 & \dots & 0 & 0 \end{pmatrix}. \tag{C10}$$

APPENDIX D: ANALYTICAL SOLUTION FOR A FOUR-TERMINAL DEVICE

In this appendix an analytical solution for the transmission between leads of a four-terminal device described by a

tight-binding Hamiltonian is presented. The system consists of five regions: four leads and a central scattering region. Assuming that leads only interact with the center region, the Hamiltonian of the device is

$$\boldsymbol{H} = \begin{pmatrix} H_1 & 0 & 0 & 0 & \tau_1^+ \\ 0 & H_2 & 0 & 0 & \tau_2^+ \\ 0 & 0 & H_3 & 0 & \tau_3^+ \\ 0 & 0 & 0 & H_4 & \tau_4^+ \\ \tau_1 & \tau_2 & \tau_3 & \tau_4 & H_C \end{pmatrix}, \tag{D1}$$

where H_i is the Hamiltonian of lead i ($i \in \{1,2,3,4\}$), and τ_i is the Hamiltonian matrix that couples lead i to the central region C. Lead i is kept at a potential $\boldsymbol{V}_i$. Considering on-site elements $2t$ and connecting elements $-t$, the Hamiltonian of the central region is

$$H_C = \begin{pmatrix} 2t+V_1 & 0 & 0 & 0 & -t \\ 0 & 2t+V_2 & 0 & 0 & -t \\ 0 & 0 & 2t+V_3 & 0 & -t \\ 0 & 0 & 0 & 2t+V_4 & -t \\ -t & -t & -t & -t & 4t+V_C \end{pmatrix}. \tag{D2}$$

The Hamiltonian of the lead i is an infinite tridiagonal matrix,

$$H_i = \begin{pmatrix} 2t+V_i & -t & 0 & 0 \\ -t & 2t+V_i & -t & 0 \\ 0 & -t & 2t+V_i & \dots \\ 0 & 0 & \dots & \dots \end{pmatrix}. \tag{D3}$$

The connection matrices τ_i have one nonzero element, $-t$, located in the final column of row i, for example,

$$\tau_3 = \begin{pmatrix} \dots & 0 & 0 \\ \dots & 0 & 0 \\ \dots & 0 & -t \\ \dots & 0 & 0 \\ \dots & 0 & 0 \end{pmatrix}. \tag{D4}$$

The self-energy of a lead i is

$$\Sigma_i = \tau_i g_i \tau_i^+. \tag{D5}$$

The Green's function of the lead is

$$g_i = \frac{E-V_i}{2t^2} - \frac{i}{2}\sqrt{1 - \frac{(E-V_i-2t^2)^2}{4t^2}} = \frac{e^{-i\phi_i}}{t}, \tag{D6}$$

where

$$\phi_i = \arccos\left(\frac{E-V_i-2t}{2t}\right). \tag{D7}$$

With these definitions, the self-energy matrices Σ_i are 5×5 and contain only one nonzero element $te^{-i\phi_i}$ located on the diagonal at (i,i). For example,

$$\Sigma_2 = \begin{pmatrix} 0 & 0 & 0 & 0 & 0 \\ 0 & te^{-i\phi_2} & 0 & 0 & 0 \\ 0 & 0 & 0 & 0 & 0 \\ 0 & 0 & 0 & 0 & 0 \\ 0 & 0 & 0 & 0 & 0 \end{pmatrix}. \tag{D8}$$

The Green's function for the central region is

$$G_C(E) = \frac{1}{E - H_C - \Sigma_1 - \Sigma_2 - \Sigma_3 - \Sigma_4}. \tag{D9}$$

With these definitions the Green's function is

$$G_C(E) = \begin{pmatrix} a_1 & 0 & 0 & 0 & -t \\ 0 & a_2 & 0 & 0 & -t \\ 0 & 0 & a_3 & 0 & -t \\ 0 & 0 & 0 & a_4 & -t \\ -t & -t & -t & -t & E-4t-V_C \end{pmatrix}^{-1} \tag{D10}$$

where $a_i = E - 2t - V_i - te^{-t\phi_i}$. The Green's function can be written in the following block form:

$$G_C = \begin{pmatrix} A & T^+ \\ T & B \end{pmatrix}^{-1} \tag{D11}$$

where

$$A = \begin{pmatrix} a_1 & 0 & 0 & 0 \\ 0 & a_2 & 0 & 0 \\ 0 & 0 & a_3 & 0 \\ 0 & 0 & 0 & a_4 \end{pmatrix}, \tag{D12}$$

$$T = -(t\ t\ t\ t) \quad \text{and} \quad B = (E - 4t - V_C). \tag{D13}$$

The inverse of block matrix can be found by partitioning[55] [see also Eq. (B5)]

$$G_C = \begin{pmatrix} A^{-1} + A^{-1}T^+ST A^{-1} & -A^{-1}T^+S \\ -ST A^{-1} & S \end{pmatrix}, \tag{D14}$$

where S is the inverse of the Schur compliment of A,

$$S = (B - TA^{-1}T^+)^{-1}. \tag{D15}$$

Since A is diagonal,

$$A^{-1} = \begin{pmatrix} f_1 & 0 & 0 & 0 \\ 0 & f_2 & 0 & 0 \\ 0 & 0 & f_3 & 0 \\ 0 & 0 & 0 & f_4 \end{pmatrix} \tag{D16}$$

where $f_i = a_i^{-1}$. With the previous definitions,

$$S = \left[E - 4t - V_C - t^2 \sum_{i=1}^{n=4} f_i\right]^{-1}. \tag{D17}$$

From this point forward S is referred to as s to reflect the fact that it is a scalar. We can now calculate elements of the Green's function explicitly,

$$G_C = \begin{pmatrix} d_1 & F_{12} & F_{13} & F_{14} & stf_1 \\ F_{21} & d_2 & F_{23} & F_{24} & stf_2 \\ F_{31} & F_{32} & d_3 & F_{34} & stf_3 \\ F_{41} & F_{42} & F_{43} & d_4 & stf_4 \\ stf_1 & stf_2 & stf_3 & stf_4 & s \end{pmatrix}, \tag{D18}$$

where $d_i = f_i + st^2 f_i^2$ and $F_{ij} = st^2 f_i f_j$. The expression for the transmission between two leads is

$$T_{ij} = \mathrm{Tr}[\Gamma_i G_C^+ \Gamma_j G_C], \tag{D19}$$

where

$$\Gamma_i = i[\Sigma_i - \Sigma_i^+]. \tag{D20}$$

The structure of Γ_i is sparse. There is only one nonzero element, $r_i = -2t \sin\phi_i$, located at (i,i). Now consider $\Gamma_j G$. The effect of multiplying by Γ_j is to pick out row j from G.

For example,

$$\Gamma_2 G^+ = \begin{pmatrix} 0 & \dots & 0 \\ r_2 G^+_{21} & \dots & r_2 G^+_{25} \\ 0 & \dots & 0 \\ \vdots & & \vdots \\ 0 & \dots & 0 \end{pmatrix}. \tag{D21}$$

Multiplying the terms and taking the trace gives

$$T_{ij} = 4t^2 \sin\phi_i \sin\phi_j \left| F_{ij} \right|^2 \tag{D22}$$

for $i \neq j$. Note that this expression is general and holds for any number of leads.

[1] C. Joachim, J. K. Gimzewski, and A. Aviram, Nature **408**, 541 (2000).
[2] A. Aviram and M. A. Ratner, Chem. Phys. Lett. **29**, 277 (1974).
[3] M. A. Reed, C. Zhou, C. J. Muller, T. P. Burgin, and J. M. Tour, Science **278**, 252 (1997).
[4] T. Sekitani, U. Zschieschang, H. Klauk, and T. Someya, Nat. Mater. **9**, 1015 (2010).
[5] R. de Picciotto, H. L. Stormer, L. N. Pfeiffer, K. W. Baldwin, and K. W. West, Nature **411**, 51 (2001).
[6] H. Song *et al.*, Nature **462**, 1039 (2009).
[7] S. V. Faleev, F. Léonard, D. A. Stewart, and M. van Schilfgaarde, Phys. Rev. B **71**, 195422 (2005).
[8] J. J. Palacios, A. J. Pérez-Jiménez, E. Louis, E. SanFabián, and J. A. Vergés, Phys. Rev. Lett. **90**, 106801 (2003).
[9] K. Stokbro, J. Taylor, M. Brandbyge, J. L. Mozos, and P. Ordejn, Comput. Mater. Sci. **27**, 151 (2003).
[10] E. G. Emberly and G. Kirczenow, Phys. Rev. B **64**, 235412 (2001).
[11] J. Taylor, H. Guo, and J. Wang, Phys. Rev. B **63**, 245407 (2001).
[12] M. B. Nardelli, J.-L. Fattebert, and J. Bernholc, Phys. Rev. B **64**, 245423 (2001).
[13] Y. Xue, S. Datta, and M. A. Ratner, J. Chem. Phys. **115**, 4292 (2001).
[14] K. Thygesen and K. Jacobsen, Chem. Phys. **319**, 111 (2005).
[15] S.-H. Ke, H. U. Baranger, and W. Yang, Phys. Rev. B **70**, 085410 (2004).
[16] P. A. Derosa and J. M. Seminario, J. Phys. Chem. B **105**, 471 (2001).
[17] S. Sanvito, C. J. Lambert, J. H. Jefferson, and A. M. Bratkovsky, Phys. Rev. B **59**, 11936 (1999).
[18] E. K. U. Gross and W. Kohn, Phys. Rev. Lett. **55**, 2850 (1985).
[19] K. Varga, Phys. Rev. B **81**, 045109 (2010).
[20] N. Sergueev, L. Tsetseris, K. Varga, and S. Pantelides, Phys. Rev. B **82**, 073106 (2010).
[21] T. Jayasekera and J. W. Mintmire, Nanotechnology **18**, 424033 (2007).
[22] C. Ritter, M. Pacheco, P. Orellana, and A. Latge, J. Appl. Phys. **106**, 104303 (2009).
[23] K. K. Saha, W. Lu, J. Bernholc, and V. Meunier, J. Chem. Phys. **131**, 164105 (2009).
[24] K. Kazymyrenko and X. Waintal, Phys. Rev. B **77**, 115119 (2008).
[25] S. Ami and C. Joachim, Phys. Rev. B **65**, 155419 (2002).
[26] H. U. Baranger, D. P. DiVincenzo, R. A. Jalabert, and A. D. Stone, Phys. Rev. B **44**, 10637 (1991).
[27] K. K. Saha, W. Lu, J. Bernholc, and V. Meunier, Phys. Rev. B **81**, 125420 (2010).
[28] M. Büttiker, Phys. Rev. Lett. **57**, 1761 (1986).
[29] P. Brusheim, D. Csontos, U. Zülicke, and H. Q. Xu, Phys. Rev. B **78**, 085301 (2008).
[30] S. K. Maiti, Solid State Commun. **150**, 1269 (2010).
[31] D. M. Cardamone, C. A. Stafford, and S. Mazumdar, Nano Lett. **6**, 2422 (2006).
[32] K. Varga and S. T. Pantelides, Phys. Rev. Lett. **98**, 076804 (2007).
[33] J. A. Driscoll and K. Varga, Phys. Rev. B **78**, 245118 (2008).
[34] J. A. Driscoll and K. Varga, Phys. Rev. B **81**, 115412 (2010).
[35] J. Taylor, *Scattering Theory* (John Wiley and Sons, New York, 1972).
[36] S. Datta, *Electronic Transport in Mesoscopic Systems* (Cambridge University Press, 1997).
[37] M. Di Ventra, *Electrical Transport in Nanoscale Systems* (Cambridge University Press, 2008).
[38] R. Kosloff and D. Kosloff, J. Comput. Phys. **63**, 363 (1986).
[39] W. H. Miller, Acc. Chem. Res. **26**, 174 (1993).
[40] T. Seideman and W. H. Miller, J. Chem. Phys. **96**, 4412 (1992).
[41] J. Muga, J. Palao, B. Navarro, and I. Egusquiza, Phys. Rep. **395**, 357 (2004).
[42] A. Vibok and G. G. Balint-Kurti, J. Phys. Chem. **96**, 8712 (1992).
[43] S. Brouard, D. Macias, and J. G. Muga, J. Phys. A **27**, L439 (1994).
[44] G. Jolicard and J. Humbert, Chem. Phys. **118**, 397 (1987).
[45] D. E. Manolopoulos, J. Chem. Phys. **117**, 9552 (2002).
[46] J. A. Driscoll and K. Varga, Phys. Rev. B **78**, 245118 (2008).
[47] T. M. Henderson, G. Fagas, E. Hyde, and J. C. Greer, J. Chem. Phys. **125**, 244104 (2006).
[48] M. P. L. Sancho, J. M. L. Sancho, and J. Rubio, J. Phys. F **15**, 851 (1985).
[49] J. Velev and W. Butler, J. Phys. Condens. Matter **16**, R637 (2004).
[50] T. P. Grozdanov and R. McCarroll, J. Phys. B **29**, 3373 (1996).
[51] V. A. Mandelshtam and H. S. Taylor, J. Chem. Phys. **103**, 2903 (1995).
[52] H. Guo, J. Chem. Phys. **108**, 2466 (1998).
[53] D. Xu, D. Xie, and H. Guo, J. Chem. Phys. **116**, 10626 (2002).
[54] F. Bouakline, T. P. Grozdanov, L. Andric, and R. McCarroll, J. Chem. Phys. **122**, 044108 (2005).
[55] W. Press, S. Teukolsky, W. Vetterling, and B. Flannery, *Numerical Recipes in C* (Cambridge University Press Cambridge, 1992).